J. Electrochem. Sci. Eng. **16** (2026) 3632; https://doi.org/10.5599/jese.3632

Open Access : : ISSN 1847-9286
https://pub.iapchem.org/ojs/index.php/JESE

Original scientific paper

One interface, two signals: excited-state lifetime shortening and electrochemical enhancement in GO-rhodamine B composites

Mansi Dhingra✉, Parul Yadav, Kashish Mishra and Saniya

Department of Physics, Maitreyi College, University of Delhi, New Delhi, India

Corresponding Authors: ✉*mdhingra@maitreyi.du.ac.in*

Received: August 4, 2026; Accepted: October 7 16, 2026; Published: October 31, 2026

Abstract

Electrochemical exfoliation of graphite rods is performed in a controlled environment to obtain graphene oxide (GO) suspensions. Graphite serves as the anode in an electrochemical cell containing H_2SO_4, NaOH and $Na_2S_2O_4$ electrolytes; the exfoliated material is collected, rinsed with deionised water and examined by Fourier-transform infrared spectroscopy, which confirms the oxygen functionalities characteristic of GO. GO-rhodamine B (RhB) composites at different GO:RhB mass ratios were characterised by steady-state photoluminescence (PL), time-resolved photoluminescence (TRPL) and cyclic voltammetry (CV). Under 520 nm excitation, where GO absorbs strongly and RhB is excited only on the short-wavelength shoulder of its $S_0 \rightarrow S_1$ band, bare GO shows strong visible PL from radiative recombination at oxygen-defect states. Progressive addition of RhB quenches this GO-centred emission and shifts the residual emission from 580 nm to 607-613 nm. TRPL shows that the emission lifetime shortens systematically with RhB loading, giving an apparent excited-state deactivation rate constant of up to $2.9\times10^8\ s^{-1}$ and demonstrating that the GO excited state is dynamically deactivated by RhB. The steady-state quenching exceeds the lifetime quenching, indicating an additional static (ground-state-association) component consistent with π-π adsorption of RhB on GO. CV of composite-modified electrodes shows substantially higher currents than the RhB-modified electrode; the 1:1 sample also shows a new quasi-reversible couple, with a cathodic peak at about +0.39 V (about -25 μA) and an anodic peak at about +0.72 V (about 40 μA). The separation of ΔEp ≈ 0.33 V is large for a scan at 30 mV s^{-1}, indicating slow electron transfers typical of an adsorbed species on conducting GO. A single band-alignment framework in which GO-to-RhB excited-state transfer (photoinduced electron transfer and/or Förster energy transfer) and GO-mediated electrode coupling arise from the same interfacial π-orbital overlap is proposed and shown to be consistent with all three datasets; the electron-versus-energy-transfer distinction is identified as requiring transient absorption spectroscopy. This work addresses an under-explored regime, distinct from the predominant literature in which GO quenches RhB fluorescence under RhB-centred excitation.

Keywords
Exfoliated graphite; fluorescent dye; photoluminescence quenching; time-resolved photoluminescence; charge transfer; cyclic voltammetry; band theory; photoinduced electron transfer

Introduction

Carbon-based nanomaterials represent one of the most intensively studied families of functional materials in contemporary materials chemistry, owing to the extraordinary diversity of electronic, optical, mechanical, and catalytic properties accessible through compositional and structural variation [1,2]. Among them, graphene, a single-atom-thick sheet of sp^2-hybridised carbon arranged in a honeycomb lattice, has attracted particular attention since its experimental isolation in 2004. However, its zero electronic bandgap (a consequence of linear π-π* band crossing at the Dirac points in the hexagonal Brillouin zone) limits its direct utility in photonic applications that require light emission [3,4]. Graphene oxide (GO), the chemically oxidised derivative of graphene, overcomes this limitation by introducing a mixture of sp^2-hybridised graphitic islands within an sp^3-hybridised, oxygen-functionalised matrix [5,6]. The lateral confinement of these sp^2 domains opens a finite, composition-dependent optical bandgap and generates a rich landscape of localised electronic states associated with oxygen functional groups (epoxy, hydroxyl, carbonyl, carboxyl), yielding a material that is intrinsically photoluminescent across the visible and near-infrared spectrum [7,8].

The photoluminescence of GO has been extensively studied and attributed to two primary mechanisms: radiative recombination of electron-hole pairs confined within quantum-sized sp^2 carbon clusters (producing an excitation-wavelength-dependent emission characteristic of a distribution of cluster sizes) [9,10], and emission mediated by oxygen-derived defect and trap states within the bandgap of the sp^2 clusters [11,12]. The relative contributions of these pathways depend on the degree of oxidation, the concentration and type of oxygen functional groups, and the excitation wavelength [13]. Critically, GO absorbs broadly across the UV and visible spectrum due to its continuous density of states, making it an efficient light-harvesting antenna even at wavelengths where conventional organic dyes absorb weakly. This broadband absorption, combined with tuneable emission and solution processability, has made GO-derived materials attractive for bioimaging, photosensing, photocatalysis, and electrochemical sensing applications [14,15].

Rhodamine B (RhB) is a xanthene dye with a well-defined, narrow $S_0 \rightarrow S_1$ absorption band cantered near 553 nm in aqueous solution (molar absorption coefficient ~100 μL mol^{-1} cm^{-1}) and strong photoluminescence near 575 to 580 nm. Its photostability, commercial availability, and thoroughly characterised ground- and excited-state redox properties (HOMO at approximately -5.6 eV *vs*. vacuum, LUMO at approximately -3.5 to -3.7 eV *vs*. vacuum) have made it a benchmark chromophore in studies of energy transfer [16], photocatalytic degradation [17], and electrochemical sensing [18]. The electrochemical redox couple of RhB ($RhB^{\cdot+}$/RhB, $E^\circ \approx +0.9$ V *vs*. Ag/AgCl) is well-resolved by cyclic voltammetry, making it a convenient probe of charge-transfer dynamics at electrode surfaces [19,20].

The interaction between GO and RhB has been the focus of numerous studies, predominantly motivated by two themes: photocatalytic degradation and fluorescence-based sensing. In photocatalytic applications, GO-based composites promote the oxidative degradation of RhB under visible-light irradiation through reactive oxygen species generated at the semiconductor-GO interface [21,22]. In fluorescence-sensing applications, the prevailing paradigm exploits GO as a "dark quencher" of RhB emission [23,24]. In this configuration, RhB (often tethered to a recognition element such as a DNA aptamer) adsorbs onto GO via π-π stacking and electrostatic interactions, and its fluorescence is quenched by a combination of Förster resonance energy transfer (FRET) and

(cc) BY

photoinduced electron transfer (PET) from the excited RhB to the broad acceptor continuum of the GO conduction band [25]. A target analyte competes for the GO surface, releases the RhB-labelled probe, and restores fluorescence—a simple, sensitive, and reagent-free detection scheme that has been applied to nucleic acid detection, heavy metal sensing, and enzyme activity assays [26].

A crucial feature common to all GO-as-quencher studies is that the excitation wavelength is tuned to match the RhB absorption maximum (~540 to 560 nm), deliberately making RhB the primary chromophore. In this regime, energy and electron flow in the direction RhB → GO. The photophysical role of GO is passive: it accepts excitation energy or electrons but does not contribute its own emission to the signal [27]. This design choice is natural for sensing but leaves a complementary regime largely unexplored: what occurs when GO, rather than RhB, is the predominant absorber? At 520 nm, RhB is excited on the short-wavelength shoulder of its $S_0 \rightarrow S_1$ band, where its molar absorption coefficient is substantially lower than at the 553 nm maximum, whereas GO absorbs through its continuous $\pi \rightarrow \pi^*$ and $n \rightarrow \pi^*$ manifold [28,29]. Excitation at 520 nm therefore does not eliminate RhB absorption, but it shifts the balance of excited-state population toward GO, particularly at high GO:RhB mass ratios. In this predominantly GO-centred regime, the roles of the two components are expected to invert: GO becomes the primary emitter, and RhB the downstream acceptor of excitation energy and/or electrons, so that the direction of photophysical flow is GO → RhB. Establishing that this inversion actually occurs, rather than assuming it from the absorption spectra, requires a kinetic probe of the GO excited state, which is the role of the time-resolved measurements introduced in this work.

The electrochemical behaviour of GO-RhB composites in the context of correlating with their optical properties has received very limited systematic treatment [30,31]. The electrochemistry of bare GO is well established: its broad, accessible density of states contributes a large double-layer capacitance and redox-active oxygen functional groups produce Faradaic features; the conductive sp^2 network provides electronic pathways for current collection [32]. Bare RhB, conversely, exhibits modest electrochemical activity from its narrow HOMO-LUMO system and shows low current when physisorbed onto an electrode without a conductive scaffold [33,34]. When GO and RhB are combined, one anticipates that the GO scaffold will wire RhB electronically to the electrode surface, while the interfacial states formed by GO-RhB coupling will introduce additional density of states accessible to the electrode. Both effects should produce higher current in composites than in bare RhB. A composition-resolved study of how CV current evolves across the GO-RhB composite series, correlated mechanistically with the optical quenching behaviour, has not been reported [35].

In this work, we address this gap by (i) preparing GO-RhB composites over a range of mass ratios, (ii) characterising their steady-state PL and excited-state lifetimes under 520 nm excitation and (iii) performing CV measurements on composite-modified glassy carbon electrodes. We show that the GO-centred PL emission is systematically quenched and red-shifted by RhB, that the emission lifetime shortens with RhB loading in a manner consistent with dynamic deactivation of the GO excited state by RhB, that bare RhB is the weakest sample under these conditions, and that composite-modified electrodes carry markedly higher current than bare RhB. These observations are rationalised within a single band-alignment framework based on GO → RhB excited-state transfer; we are careful to distinguish what the present data establish (the existence of a dynamic quenching channel) from what they leave open (the relative contributions of electron transfer and Förster energy transfer), and we identify the additional measurement needed to close that gap [36,37].

Experimental

Materials

Graphite rods (2 mm diameter, 99 %), sodium thiosulfate ($Na_2S_2O_3$, ≥99 %), concentrated sulfuric acid (H_2SO_4, 95 to 98 %), sodium hydrosulfite ($Na_2S_2O_4$), sodium hydroxide (NaOH) and rhodamine B (RhB, dye content ≥95 %) were purchased from Sigma-Aldrich and used as received. All solutions were prepared with deionised water (≥18.2 MΩ cm, Millipore Milli-Q).

Synthesis of graphene oxide

All graphene oxide samples employed in this study were synthesised in the laboratory by electrochemical exfoliation. High-purity graphite rods served as working and counter electrodes; NaOH (0.1 M), H_2SO_4 (0.5 M), $Na_2S_2O_3$ (trace) and $Na_2S_2O_4$ (1 M) in deionised water served as electrolytes. All chemicals were of analytical grade unless otherwise specified.

Electrochemical exfoliation

Exfoliation was carried out in a two-electrode cell in which a graphite rod (2×70 mm) served as the anode and an identical graphite rod as the cathode; we used anode/cathode rather than working/counter terminology because no reference electrode was present. The rods were mounted parallel, 4 cm apart, with an immersed length of 5 cm in 100 mL of electrolyte in a 250 mL beaker at [25 ± 2] °C without external cooling. A constant voltage of 15 V was applied from a DC power supply; the current was 20 mA initially and rose to 219 mA over the 7 min run as the anode expanded and exfoliated. The exfoliated material was collected by filtration, washed with deionised water at least three times until the washings reached pH 6.5-7, and vacuum-dried at 80 °C for 12 h. Voltage, spacing and duration were fixed from preliminary optimisation and literature precedent.

The electrolyte composition was varied to examine the effect of acid, base, salt and aqueous solvent on intercalation, expansion and exfoliation (Table 1). Systems 1 and 2 differ in the presence of an accelerator that supports the exfoliation process.

Table 1. *Electrolyte systems used for electrochemical exfoliation*

Electrolyte system	Composition	Purpose
System 1 (S1)	NaOH (0.1 M) + H_2SO_4 (0.5 M) + $Na_2S_2O_3$ (trace) + deionised water	Acid-base combined intercalation and ion interaction
System 2 (S2)	$Na_2S_2O_4$ (1 M) + H_2SO_4 (0.5 M) + deionised water	Salt-acid system and aqueous-solvent effect

Preparation of graphene oxide-rhodamine B composites

GO was dispersed in deionised water (5 mg mL^{-1}) by 30 min probe sonication. RhB stock solutions (10^{-3} M in deionised water) were prepared separately. Composites at GO:RhB mass ratios of 10:1, 5:1, 2:1 and 1:1 were produced by combining appropriate volumes of the two stocks under magnetic stirring (12 h, room temperature). The GO sample used for all composites was S2. The final RhB concentration in the composite dispersions was 1 mM. The resulting dispersions were colloidally stable for at least 72 h and used directly for characterisation.

Characterization

Steady-state PL spectra were recorded on a combined steady-state and time-resolved fluorescence spectrometer (Model: F900) manufactured by Edinburgh Instruments, UK (λ_{ex} = 520 nm, slit width 5 nm) at room temperature (25±2 °C) in 1 cm quartz cuvettes; all samples were measured on

CC BY

the same day with identical instrument settings so that intensities are directly comparable. FTIR transmission spectra were collected on a Thermo Scientific Nicolet iS50, USA spectrometer.

Electrochemical measurements

Cyclic voltammetry was performed using an OrigaFlex OGF500 potentiostat in a conventional three-electrode cell: glassy carbon working electrode (GCE), 3 mm diameter, geometric area 0.0707 cm^2), platinum wire counter electrode and Ag/AgCl (3 M KCl) reference electrode. Before each modification, the GCE was polished with 0.3 and 0.05 µm alumina slurry, rinsed with water and ethanol and dried. Working electrodes were prepared by drop-casting 5 µL of dispersion on the polished GCE and drying for 2 h. Working electrodes were prepared from all four composite dispersions (10:1, 5:1, 2:1 and 1:1), from a bare RhB solution, and from the GO dispersion to provide a reference for the contribution of the GO scaffold alone. The RhB-containing electrodes all contain RhB at 1 mM so that the RhB loading is identical on every composite electrode. CV scans were recorded in 0.1 M phosphate-buffered saline (PBS, pH 7.0) at 30 mV s^{-1} from -1.0 to +1.0 V *vs*. Ag/AgCl, after purging with N_2 for 10 min. Scans were initiated at the open-circuit potential and five complete cycles (-1.0 → +1.0 → -1.0 V) were recorded for each electrode. Because the first negative-going sweep is systematically 10 to 15 % larger than the following sweeps (reduction of surface oxygen functionalities on the first scan), the currents reported in Table 4 are the mean ± SD, calculated from the three negative-going (cathodic) sweeps and three positive-going (anodic) sweeps corresponding to cycles 3 to 5.

Time-resolved photoluminescence

Fluorescence decay curves were acquired by time-correlated single-photon counting on a time-resolved fluorescence spectrometer (Model: F900) manufactured by Edinburgh Instruments, equipped with time-correlated single-photon counting (TCSPC) using a 520 nm pulsed diode laser and detecting at the emission maximum of each sample at 580 nm.

Uncertainty and reproducibility

TRPL decays were fitted using OriginPro software (https://www.originlab.com/) with a single-exponential model $I(t) = A \cdot \exp(-t/\tau) + B$, where τ is the carrier lifetime. Fit quality was assessed by reduced χ^2 (threshold ≤ 1.2). All lifetimes are the mean of two independent sample preparations. All CV data are reported as mean±SD, calculated from the three negative-going (cathodic) sweeps and three positive-going (anodic) sweeps corresponding to cycles 3 to 5. The first two cycles were used as conditioning cycles and excluded from the analysis.

Results and discussion

Fourier-transform infrared spectroscopy analysis

The Fourier-transform infrared (FTIR) spectra were analysed to identify the characteristic absorptions of O-H, COOH, C=O, C-O-C and C=C groups. The spectra of S1 and S2 (Figure 1) exhibit the oxygen-containing functionalities associated with oxidised graphene-based materials. The broad band near 3286 cm^{-1} is assigned to O-H stretching, the absorption near 2947 cm^{-1} to sp^3 C-H stretching, the band near 1627 cm^{-1} to C=C skeletal vibration, and the peaks near 1196 and 1052 cm^{-1} to C-O-C and C-O stretching, respectively. The degree of oxidation can be estimated from the ratio of the oxygen-related peak intensity to the C=C peak intensity, Equation (1):

Relative oxidation ∝ oxygen functional group peak intensity / C=C peak intensity

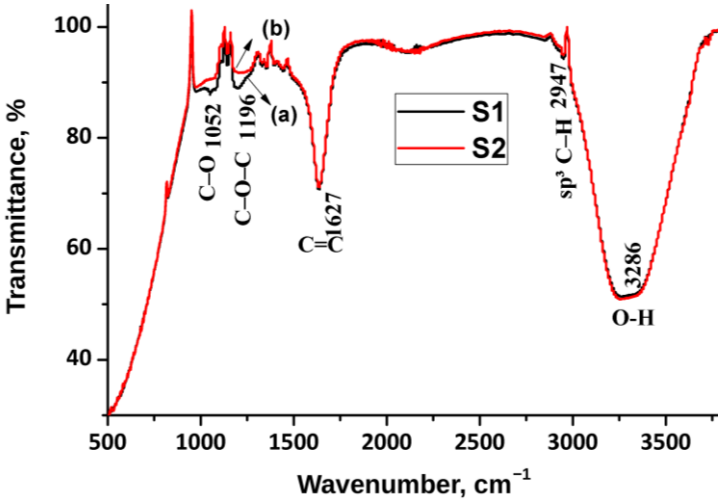


Figure 1. *FTIR spectra of (a) System 1 and (b) System 2*

A relative oxidation ratio below 1 indicates that graphitic carbon dominates and oxidation is low; a ratio of 1-2 indicates moderate oxidation; a ratio above 2 indicates relatively high oxidation. Compared with S1, S2 shows slightly stronger oxygen-related absorption bands, indicating a higher degree of oxidation or surface functionalisation.

Band structure of GO and its photoluminescence mechanism

Understanding the optical and electrochemical behaviour of GO-RhB composites requires a firm grounding in the band structure of each component. Pristine graphene is a zero-bandgap semimetal: its π and π* bands meet at the Dirac points (K and K′ points of the hexagonal Brillouin zone), yielding a linear dispersion and no finite bandgap. Consequently, pristine graphene is non-emissive in the visible spectrum. GO, by contrast, is electronically heterogeneous: sp^2-hybridised carbon atoms form isolated graphitic islands (estimated diameter 1-5 nm in typical Hummers-derived GO) embedded within a continuous sp^3-hybridised, oxygen-functionalised network. Quantum confinement of π-electrons within these sp^2 clusters opens a finite optical bandgap whose magnitude scales inversely with cluster size, analogous to zero-dimensional carbon quantum dots. The resulting electronic structure features a pseudo-conduction band (π* states of sp^2 clusters) separated from a pseudo-valence band (π states) by a distribution of gap energies reflecting the cluster-size polydispersity. This accounts for the excitation-wavelength dependence of GO emission: different excitation wavelengths preferentially populate sp^2 clusters of different sizes, each emitting at a characteristic Stokes-shifted wavelength.

Within this bandgap, oxygen functional groups-specifically carbonyl (C=O) and hydroxyl (C-OH) groups at sp^2 cluster edges, and epoxy (C-O-C) groups on the basal plane introduce localised electronic states commonly termed defect or trap states. These trap states, typically lying 0.3 to 1.5 eV below the π* band minimum, serve as efficient relaxation intermediates: photoexcited electrons in the π* band rapidly relax (picosecond timescale) into the nearest available trap state before undergoing slower (nanosecond) radiative recombination to the π valence band. This trap-state-mediated recombination is responsible for the broad, Stokes-shifted PL emission characteristic of GO, which persists from the blue to the red region of the visible spectrum depending on excitation wavelength and degree of oxidation. Figure 2 presents a schematic energy diagram of this band structure and the associated PL mechanism under 520 nm excitation.

CC BY

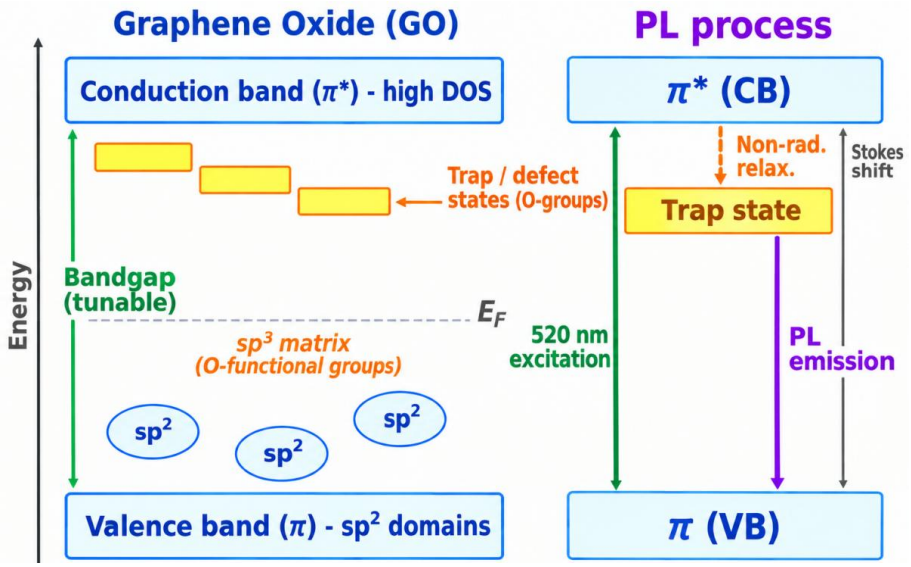


Figure 2. *Band structure of graphene oxide and photoluminescence mechanism under 520 nm excitation. The π* conduction band (CB) and π valence band (VB) are separated by a finite bandgap arising from quantum confinement in sp² carbon clusters. Oxygen-derived trap states within the gap mediate non-radiative relaxation from the CB, followed by radiative emission (PL). The Fermi level (E_F) lies within the gap. DOS = density of states*

Steady-state photoluminescence of bare graphene oxide, bare rhodamine B and graphene oxide--rhodamine B composites

The PL spectra in Figure 3, measured under 520 nm excitation, reveal a clear hierarchy of emission intensities: bare GO exhibits the strongest emission (peak at 580 nm), the composites show intermediate intensities that decrease progressively with increasing RhB content and bare RhB displays the weakest emission.

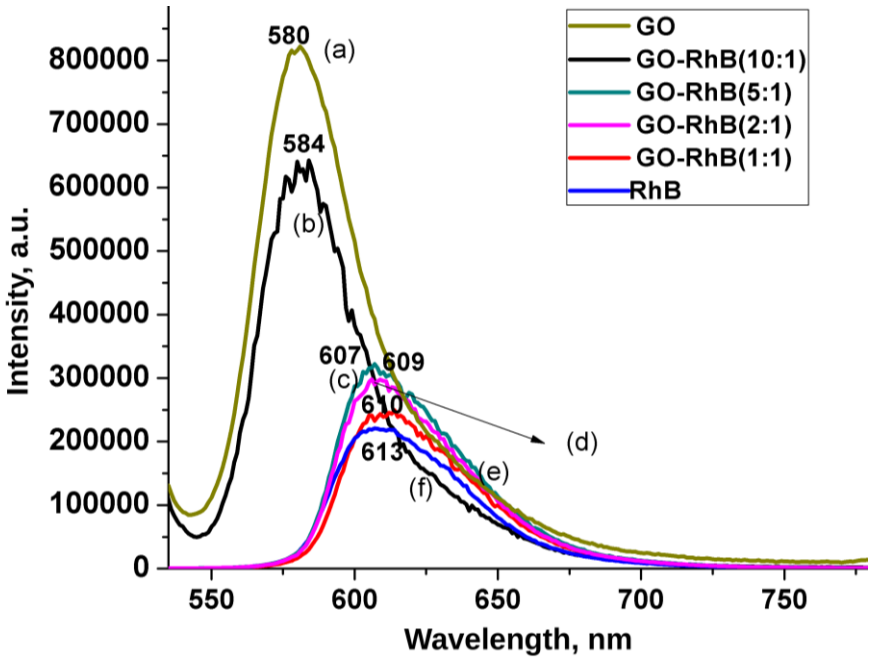


Figure 3. *PL spectra (λ_{ex} = 520 nm) of (a) GO, (b) GO-RhB (10:1), (c) GO-RhB (5:1), (d) GO-RhB (2:1), (e) GO-RhB (1:1) and (f) RhB*

Peak intensities and positions read from the spectra are collected in Table 2. The strong emission of bare GO at 580 nm reflects the efficient trap-state-mediated recombination pathway described above. The weakness of bare RhB under 520 nm excitation is a consequence of spectral mismatch:

the $S_0 \rightarrow S_1$ absorption maximum of RhB in water lies near 553 nm, so at 520 nm RhB is excited on the short-wavelength shoulder of its band with a substantially reduced (though not negligible) molar absorption coefficient, and the resulting excited-state population is small. This contrasts with the conventional GO-RhB literature, in which excitation near 550 nm makes RhB the dominant absorber and emitter. At 520 nm, the situation is largely inverted: GO is the principal absorber and emitter, and RhB acts predominantly as a downstream acceptor.

Table 2*. Steady-state PL parameters under 520 nm excitation. Intensities are peak values read from Figure 3.* I/I_0 *is the composite peak intensity relative to bare GO peak intensity (*$\lambda_{em,\,max}$ *is the wavelength of maximum emission)*

Sample (mass ratio)	$\lambda_{em,max}$ / nm	Peak intensity, a.u.	I/I_0	Ratio of intensity to bare RhB peak intensity
GO	580	8.2	1.00	3.7
GO-RhB (10:1)	584	6.4	0.78	2.9
GO-RhB (5:1)	607	3.2	0.39	1.45
GO-RhB (2:1)	609	2.9	0.35	1.3
GO-RhB (1:1)	610	2.5	0.30	1.1
RhB	613	2.2	0.27	1.00

Two spectroscopic changes accompany the introduction of RhB into the GO dispersion: a decrease in PL intensity and a red shift of the emission maximum from 580 nm to 607 to 613 nm. At the 10:1 ratio the GO band survives with reduced intensity (584 nm); from 5:1 onward, the 580 nm band is essentially removed, and the residual emission appears as a broad band at 607-613 nm whose position and envelope closely resemble those of the bare RhB spectrum under the same excitation. Both observations are consistent with formation of an electronically coupled GO-RhB interface: the loss of the 580 nm band indicates that a new deactivation channel competes with radiative trap-to-valence-band recombination in GO, and the 607 to 613 nm band can originate either from radiative decay of an interfacial charge-transfer (CT) state or from RhB emission sensitised by energy transfer from GO (or, in part, from direct excitation of RhB at 520 nm). Steady-state spectra alone cannot distinguish these possibilities, and we therefore do not treat the red shift as proof of a CT state. What the steady-state data do establish is that quenching of the GO-centred emission deepens monotonically as the GO:RhB ratio decreases (Table 2, I/I_0 = 0.78 → 0.30) and saturates between 2:1 and 1:1, consistent with progressive coverage of the GO sheets by adsorbed RhB. The kinetic character of this quenching is examined by TRPL. Figure 4 provides comparative band diagrams for the three sample categories.

Band-alignment considerations for graphene oxide-rhodamine B electron/energy transfer

Reported energy-level alignments indicate that photoinduced transfer between GO and RhB is energetically plausible, though the available data do not establish a preferred direction. The work function of GO (approximating its Fermi level) has been reported at 4.5 to 4.9 eV below vacuum, placing its π* conduction-band minimum at roughly 3.5 to 4.0 eV below vacuum. The LUMO of RhB has been reported at -3.5 to -3.7 eV *vs*. vacuum [38]. These ranges overlap substantially, and depending on where the true values for the present materials fall within them, the alignment could favour transfer in either direction. We did not attempt a quantitative Rehm-Weller estimate [39], since this requires oxidation and reduction potentials for GO that are not well-defined for this material; a calculation built on unsupported literature values would not meaningfully constrain the direction of transfer.

(cc) BY

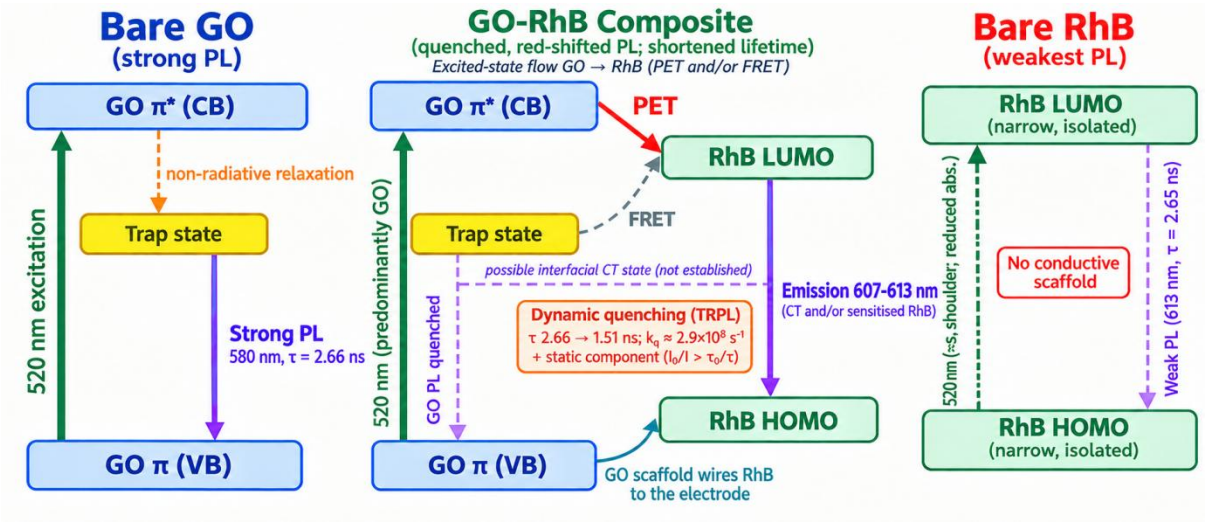


Figure 4. *Comparative band diagrams for bare GO (left), GO-RhB composite (centre) and bare RhB (right) under 520 nm excitation. In bare GO, photoexcited electrons in the π* band relax to trap states and recombine radiatively (strong PL). In the composite, GO → RhB excited-state transfer (PET and/or FRET) opens a non-radiative channel for GO (quenching) and gives rise to the red-shifted 607-613 nm band. In bare RhB, weak 520 nm absorption yields the weakest emission*

We instead treat GO-RhB transfer as energetically feasible but kinetically undetermined and rely on future transient-absorption and excitation-spectrum measurements to establish direction.

Time-resolved photoluminescence: kinetic evidence for dynamic deactivation of the graphene oxide excited state by rhodamine B

Steady-state quenching can arise either from a dynamic process that competes with emission during the excited-state lifetime (PET, FRET) or from static ground-state association that removes emitters before excitation; only the former shortens the measured lifetime [40]. TRPL therefore provides the discriminating kinetic test that the steady-state data cannot. Decay curves for GO, RhB and the four composites are shown in Figure 5 and the fitted lifetimes are listed in Table 3.

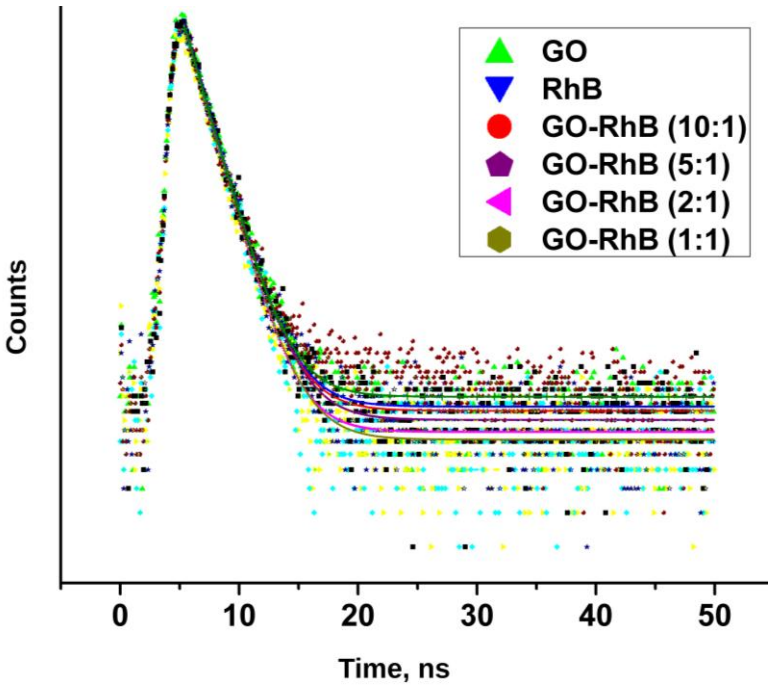


Figure 5. *TRPL decay curves (normalised) of GO, RhB and GO-RhB composites at 10:1, 5:1, 2:1 and 1:1 mass ratios, detected at 580 nm*

Table 3. *TRPL lifetimes and derived kinetic parameters. τ_o = 2.66 ns (bare GO). The last two columns compare the steady-state and lifetime-based quenching ratios (τ= carrier lifetime, τ_o=carrier lifetime for bare GO, SE = standard error, k_q=deactivation rate constant)*

c (mass ratio)	τ ± SE / ns	Adj. R^2	τ_o/τ	$\eta_{dyn} = 1 - \tau/\tau_o$	k_q / 10^8 s^{-1}	I_o/I (steady state)	$(I_o/I)/(\tau_o/\tau)$
GO	2.66 ± 0.34	0.948	1.00	-	-	1.00	1.00
GO-RhB (10:1)	2.31 ± 0.19	0.962	1.15	0.13	0.58	1.28	1.11
GO-RhB (5:1)	1.90 ± 0.08	0.992	1.40	0.29	1.50	2.56	1.83
GO-RhB (2:1)	1.57 ± 0.03	0.999	1.69	0.41	2.61	2.83	1.67
GO-RhB (1:1)	1.51 ± 0.03	0.998	1.77	0.43	2.89	3.28	1.85
RhB	2.65 ± 0.28	0.961	-	-	-	-	-

Time-resolved photoluminescence (TRPL) decays of GO, RhB and the GO-RhB composites (10:1, 5:1, 2:1 and 1:1) were recorded under identical conditions, with excitation at 520 nm, the same wavelength used for the steady-state PL and the mechanistic experiments, and detection at 580 nm for all samples. Decays were fitted with a single-exponential function, and the lifetimes are given as the fitted value ± standard error. Bare GO and bare RhB give indistinguishable lifetimes of 2.66±0.34 and 2.65±0.28 ns, respectively. A change in which of the two species dominates the signal therefore cannot by itself change the measured lifetime. On composite formation, the lifetime shortens progressively as the GO-to-RhB ratio decreases: 2.31±0.19 ns (10:1), 1.90±0.08 ns (5:1), 1.57±0.03 ns (2:1) and 1.51±0.03 ns (1:1).

These results are consistent with the formation of a ground-state charge-transfer (CT) complex between GO (electron donor) and adsorbed RhB^+ (electron acceptor). The steady-state spectra show that, with RhB held fixed, the GO band at 580 nm is almost completely quenched at 5:1 and below. The intensity at 580 nm falls by 22 to 69%, whereas the lifetime shortens by only 13 to 43%, which is the signature of predominantly static quenching, i.e., the formation of non-emissive GO-RhB CT complexes. The progressive shortening of the lifetime shows that a smaller dynamic contribution is also present, in which the CT interaction opens an additional non-radiative decay channel for the emitting species that remain. In the 5:1, 2:1 and 1:1 composites, the residual intensity at 580 nm is comparable to the blue edge of bare RhB, so the lifetimes in these samples reflect the remaining GO-RhB species and not a single, uniquely identified population. Taken together, the PL and TRPL data indicate that CT complexation quenches the emission of the GO-RhB pair, with the extent of quenching increasing with the RhB-to-GO ratio.

What TRPL alone does not settle is whether the excitation leaves GO as an electron (PET, generating $GO^{+}\cdot/RhB^{-}\cdot$) or as an exciton (FRET, generating RhB*) [41]. Both processes shorten the donor lifetime identically. We therefore describe the mechanism as GO → RhB excited-state transfer comprising PET and/or FRET, and identify the transient-absorption experiment as the necessary next step.

Electrochemical behaviour: cyclic voltammetry

CV curves (−1.0 to +1.0 V *vs.* Ag/AgCl, 30 mV s^{-1}) for the Bare GCE, GO-modified GCE, RhB-modified GCE and the 10:1, 5:1, 2:1 and 1:1 composite-modified GCEs are shown in Figure 6. The RhB-modified GCE shows low current across the whole window, with a modest Faradaic response near +0.9 V assignable to the $RhB\cdot^{+}$/RhB couple. The limited current of bare RhB reflects (i) the narrow, isolated HOMO-LUMO system of RhB, which provides few electrochemically accessible states away from its redox potential and hence little capacitive contribution, and (ii) the absence of a conductive scaffold, which leaves physisorbed RhB poorly coupled to the GCE and raises the charge-transfer resistance. Together, these factors make bare RhB electrochemically sluggish, paralleling its weak optical response at 520 nm.

(cc) BY

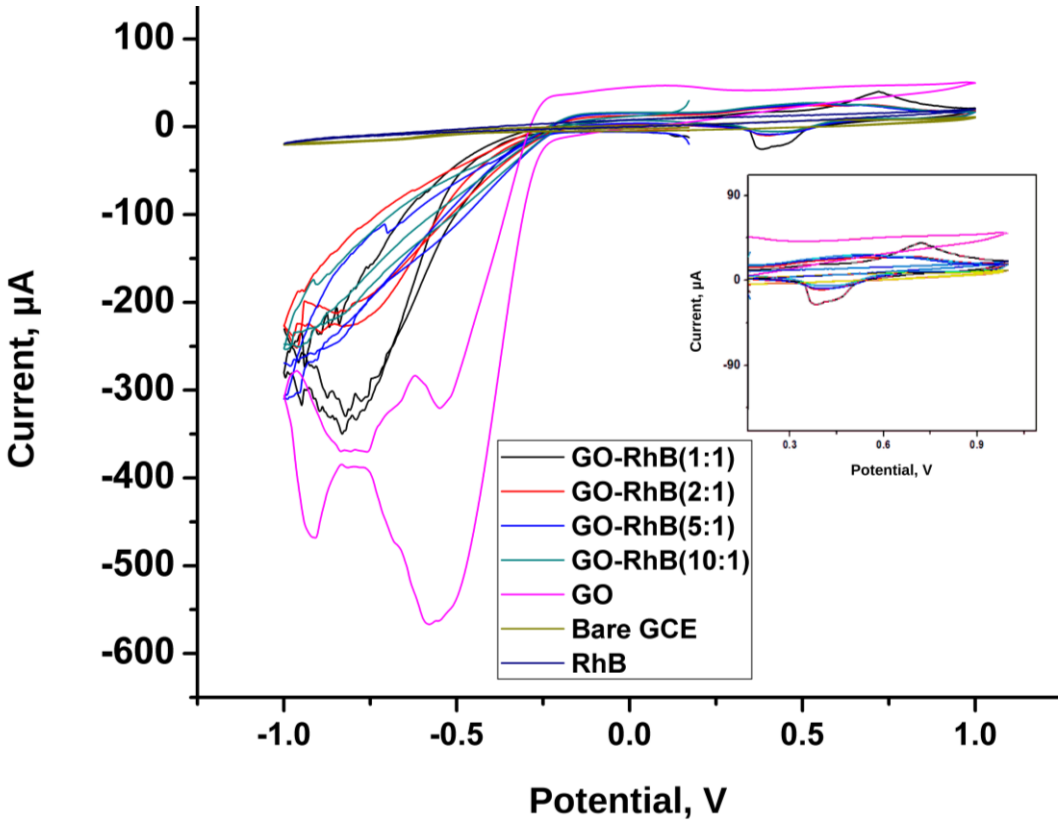


Figure 6. *Cyclic voltammograms in 0.1 M PBS (pH 7.0) at 30 mV s^{-1} of GCEs modified with bare GO, GO-RhB (10:1), (5:1), (2:1) and (1:1) composites, and bare RhB. The inset magnifies the 0.2 to 1.0 V region where the redox peaks of GO-RhB(1:1) are easier to see*

Pristine GO shows the strongest cathodic response of all samples, an irreversible reduction beginning near -0.3 V with peaks at about -0.58 V (about 570 µA) and -0.90 V (about -470 µA), plus a shoulder near -0.8 V. These peaks are assigned to the reduction of oxygen-containing groups, *viz.* epoxy and hydroxyl first, then carbonyl and carboxyl. GO has no sharp redox features in the positive region and no anodic wave on the return scan. In the 1:1 GO-RhB composite, the -0.58 V peak disappears, and the remaining GO features merge into a single, weaker peak near -0.83 V (about -350 µA). This peak is about 0.07 V less negative than the -0.90 V GO peak and about 40 % smaller in magnitude. We interpret this as electron flow from GO to adsorbed RhB^+, with electrons that would otherwise reduce GO's functional groups used instead for RhB^+ reduction at the interface. The 1:1 sample also shows a new quasi-reversible couple, with a cathodic peak at about +0.39 V (about -25 µA) and an anodic peak at about +0.72 V (about +40 µA). The separation of $\Delta E_p \approx 0.33$ V is large for a scan at 30 mV s^{-1}, indicating slow electron transfer typical of an adsorbed species on conducting GO [42]. It suggests a new electrochemically active species or a new oxidation pathway that only exists when the two components interact. The couple is absent from GO and from bare RhB, so it is attributed to the GO-RhB interface. As the GO mass increases from 1:1 to 10:1, the negative-region features become a broad, undefined cathodic current (about -230 µA at -1.0 V). In the positive region, the cathodic peak stays near +0.40 V while its current falls from about -25 µA to between -10 and -6 µA. The anodic peak weakens and shifts negatively to a broad hump near +0.6 to 0.65 V. This suggests that the GO-RhB interaction is strongest at 1:1 and is diluted at higher GO loadings, where the same amount of RhB spreads over more GO surface. Overall, the suppressed GO reduction, the merged peak, and the new composite couple that fades with increasing GO mass are consistent with GO → RhB charge transfer. The unified picture that connects the optical and electrochemical observations through a common interfacial origin, which we treat as a working hypothesis, is summarised in Figure 7.

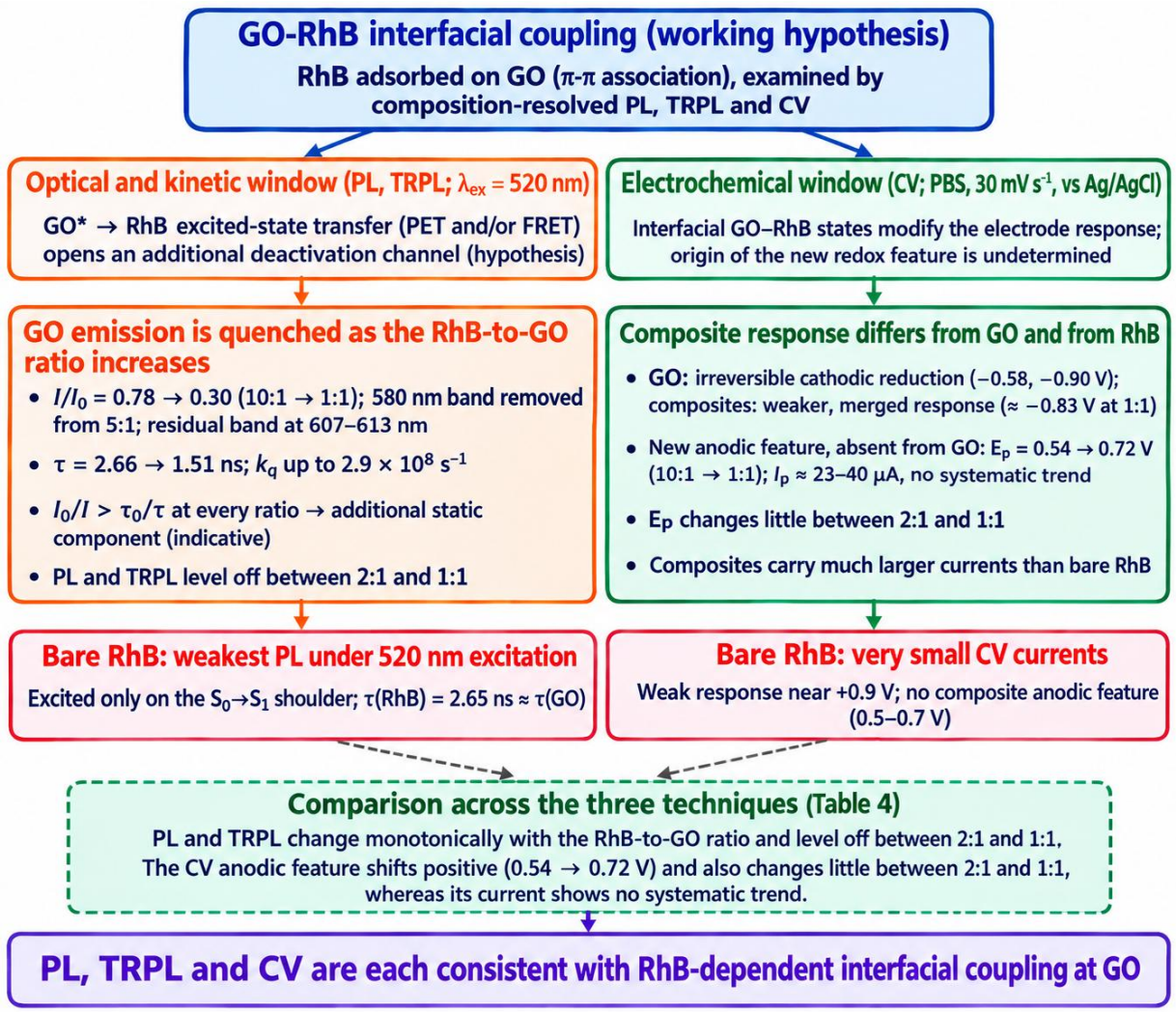


Figure 7. *Unified mechanistic picture: a single root cause, GO-RhB interfacial π-orbital coupling, simultaneously opens the GO → RhB excited-state deactivation channel (PL quenching, lifetime shortening, red-shifted residual band) and wires RhB to the electrode through the GO scaffold and interfacial states (CV enhancement). The weakness of bare RhB in both experiments follows from the same structural argument*

Direction of excited-state flow: this work versus the rhodamine B-centred literature

It is instructive to contrast the direction of excited-state flow in this work with that in the predominant GO-RhB literature (Figure 8). The existing literature uses ~550 nm excitation (RhB-centred regime), making RhB the donor and GO the acceptor (RhB → GO). In the present work, 520 nm excitation places most of the excited-state population on GO, making GO as the possible donor and RhB as the acceptor (GO → RhB). As shown above, the reported energy levels allow transfer in either direction, so the reversal does not arise from thermodynamics. It arises from which chromophore is photoexcited. The RhB-dependent shortening of the GO emission lifetime supports the GO → RhB direction under 520 nm excitation. The reversal is not merely semantic: it corresponds to a different excited-state population, different optimum compositions for maximising the effect, and different application contexts. The GO-centred regime, where GO is the primary emitter and light-harvesting antenna, is particularly relevant for GO-based photosensors and photoelectronchemical devices in which GO itself, rather than a tethered dye, acts as the chromophoric core.

CC BY

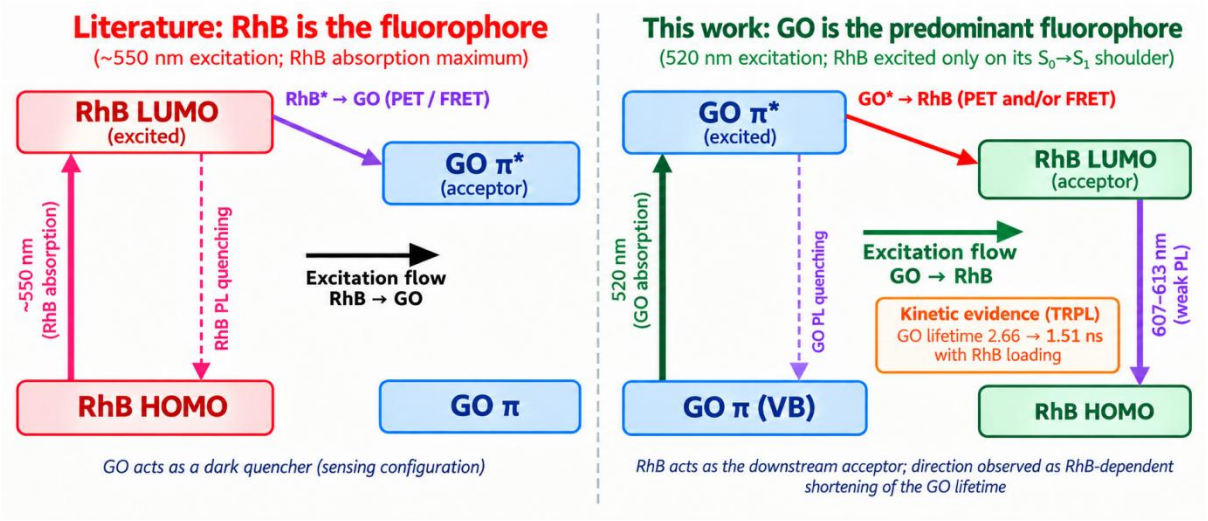


Figure 8. *Direction of excited-state flow in the literature (RhB-centred, ~550 nm excitation; RhB → GO) versus this work (predominantly GO-centred, 520 nm; GO → RhB)*

Limitations and scope of the mechanistic claims

The present data permit mechanistic claims and we state them explicitly rather than conflating them.

Established by the present dataset: Under 520 nm excitation, GO-centred emission is quenched by RhB through two co-existing channels. The dynamic channel is evidenced by systematic lifetime shortening (2.66 → 1.51 ns, Table 3) that scales monotonically with RhB loading and saturates between the 2:1 and 1:1 ratios; the apparent deactivation rate constant reaches 2.9×10^{8} s^{-1} at 1:1. The static channel is evidenced by the excess of steady-state quenching (I_o/I up to 3.3) over the lifetime ratio (τ_o/τ up to 1.8), which is the diagnostic signature of ground-state complex formation. Both channels grow with RhB content and point unambiguously to GO as the quenched donor and RhB as the acceptor under these excitation conditions, confirming the GO → RhB direction of excited-state flow. Two independent CV signatures corroborate interfacial coupling in the ground state: (i) the GO cathodic peak shifts from -0.90 to -0.83 V in the 1:1 composite consistent with partial withdrawal of electron density from the GO π-framework by adsorbed RhB^{+} and (ii) a new quasi-reversible couple appears at +0.39/+0.72 V ($\Delta E_p \approx 0.33$ V) in the 1:1 composite and is absent from bare GO and bare RhB under identical conditions, so it is assigned to an electrochemically active feature associated with the GO-RhB interface, whose origin is not yet determined. PL quenching and TRPL lifetime shortening vary monotonically with the GO to RhB ratio and level off between 2:1 and 1:1 (Table 4). The anodic feature in the CV shifts to more positive potential with increasing the ratio (0.54 → 0.72 V) and changes little between 2:1 and 1:1, whereas its current shows no systematic trend. The three techniques therefore vary in the same direction with composition, but not in step, and we regard a common interfacial origin as a hypothesis.

Table 4. *Composition dependence of the PL, TRPL and CV responses of GO-RhB composites*

Sample (mass ratio)	PL	TRPL	CV	
	I/I_o (λ / nm)	$\tau \pm$ SE / ns	Anodic E_p / V	Anodic I_p / µA
GO	1.00 (580)	2.66 ± 0.34	—	—
GO-RhB (10:1)	0.78 (584)	2.31 ± 0.19	0.54	27 to 29
GO-RhB (5:1)	0.39 (607)	1.90 ± 0.08	0.55	25 to 27
GO-RhB (2:1)	0.35 (609)	1.57 ± 0.03	0.69	23 to 25
GO-RhB (1:1)	0.30 (610)	1.51 ± 0.03	0.72	28 to 40
RhB	0.27 (613)	2.65 ± 0.28	~0.9 (weak)	-

Conclusions

This work explores a regime of GO-Rhodamine B composites that has been largely overlooked: excitation at 520 nm, where GO is the principal absorber and emitter. Steady-state PL, TRPL and cyclic voltammetry together give a consistent picture of a strongly coupled GO-RhB interface. RhB quenches the trap-state emission of GO (I/I_0 = 0.78 → 0.30 from 10:1 to 1:1), removes the 580 nm GO band from 5:1 onward and leaves a red-shifted residual band at 607 to613 nm. The emission lifetime shortens in steps, from 2.66 ns for GO to 1.51 ns at 1:1, with an apparent deactivation rate constant of up to 2.9×10^8 s^{-1}, and both PL and TRPL level off between 2:1 and 1:1. The steady-state quenching exceeds the lifetime quenching at every composition, pointing to a ground-state association between GO and RhB in addition to the dynamic channel. Electrochemically, the composites carry far larger currents than bare RhB, and a redox feature that is absent from both GO and RhB appears in the positive region, shifting from 0.54 to 0.72 V as the RhB-to-GO ratio increases and changing little between 2:1 and 1:1. These observations are consistent with a single band-alignment framework in which RhB adsorbed on GO opens an additional deactivation pathway, with GO → RhB excited-state transfer as the working hypothesis.

The three techniques vary in the same direction with composition, but not in step: the CV feature settles in the same 2:1-1:1 window as PL and TRPL, while its current shows no systematic trend. The direction of transfer, the PET/FRET distinction, the static/dynamic partition and the common origin of the optical and electrochemical responses are therefore treated as hypotheses, to be tested by femtosecond transient absorption, TRPL in the RhB emission window and replicate measurements. The GO-centred excitation regime explored here is essentially absent from the existing literature, and the combined optical-kinetic-electrochemical approach provides a route to understanding GO-dye interfaces that can be extended to other GO-dye composites for photosensing and photoelectrochemical devices.

Acknowledgements: *The authors thank the Department of Physics and Astrophysics, University of Delhi, for characterisation facilities and Maitreyi College, University of Delhi, for financial support and technical assistance.*

Funding: *This research was funded by Maitreyi College, University of Delhi.*

Conflicts of interest: *The authors declare no conflict of interest.*

References

[1] K. S. Novoselov, A. K. Geim, S. V. Morozov, D. Jiang, Y. Zhang, S. V. Dubonos, I. V. Grigorieva, A. A. Firsov, Electric field effect in atomically thin carbon films, *Science* **306** (2004) 666-669. https://doi.org/10.1126/science.1102896

[2] A. K. Geim, K. S. Novoselov, The rise of graphene, *Nature Materials* **6** (2007) 183-191. https://doi.org/10.1038/nmat1849

[3] K. F. Mak, M. Y. Sfeir, Y. Wu, C. H. Lui, J. A. Misewich, T. F. Heinz, Measurement of the optical conductivity of graphene, *Physical Review Letters* **101** (2008) 196405. https://doi.org/10.1103/PhysRevLett.101.196405

[4] R. R. Nair, P. Blake, A. N. Grigorenko, K. S. Novoselov, T. J. Booth, T. Stauber, N. M. R. Peres, A. K. Geim, Fine structure constant defines visual transparency of graphene, *Science* **320** (2008) 1308. https://doi.org/10.1126/science.1156965

[5] A. Lerf, H. He, M. Forster, J. Klinowski, Structure of graphite oxide revisited, *The Journal of Physical Chemistry B* **102** (1998) 4477-4482. https://doi.org/10.1021/jp9731821

(cc) BY

[6] D. C. Marcano, D. V. Kosynkin, J. M. Berlin, A. Sinitskii, Z. Sun, A. Slesarev, L. B. Alemany, W. Lu, J. M. Tour, Improved synthesis of graphene oxide, *ACS Nano* **4** (2010) 4806-4814. https://doi.org/10.1021/nn1006368
[7] K. P. Loh, Q. Bao, G. Eda, M. Chhowalla, Graphene oxide as a chemically tunable platform for optical applications, *Nature Chemistry* **2** (2010) 1015-1024. https://doi.org/10.1038/nchem.907
[8] G. Eda, Y.-Y. Lin, C. Mattevi, H. Yamaguchi, H.-A. Chen, I.-S. Chen, C.-W. Chen, M. Chhowalla, Blue photoluminescence from chemically derived graphene oxide, *Advanced Materials* **22** (2010) 505-509. https://doi.org/10.1002/adma.200901996
[9] J. Shang, L. Ma, J. Li, W. Ai, T. Yu, G. G. Gurzadyan, The origin of fluorescence from graphene oxide, *Scientific Reports* **2** (2012) 792. https://doi.org/10.1038/srep00792
[10] T. Gokus, R. R. Nair, A. Bonetti, M. Böhmler, A. Lombardo, K. S. Novoselov, A. K. Geim, A. C. Ferrari, A. Hartschuh, Making graphene luminescent by oxygen plasma treatment, *ACS Nano* **3** (2009) 3963-3968. https://doi.org/10.1021/nn9011897
[11] S. Zhu, J. Zhang, C. Qiao, S. Tang, Y. Li, W. Yuan, B. Li, L. Tian, F. Liu, R. Hu, H. Gao, H. Wei, H. Zhang, H. Sun, B. Yang, Strongly green-photoluminescent graphene quantum dots for bioimaging applications, *Chemical Communications* **47** (2011) 6858-6860. https://doi.org/10.1039/c1cc11122a
[12] K. Krishnamoorthy, M. Veerapandian, K. Yun, S.-J. Kim, The chemical and structural analysis of graphene oxide with different degrees of oxidation, *Carbon* **53** (2013) 38-49. https://doi.org/10.1016/j.carbon.2012.10.013
[13] X. Sun, Z. Liu, K. Welsher, J. T. Robinson, A. Goodwin, S. Zaric, H. Dai, Nano-graphene oxide for cellular imaging and drug delivery, *Nano Research* **1** (2008) 203-212. https://doi.org/10.1007/s12274-008-8021-8
[14] Y. Wang, Z. Li, J. Wang, J. Li, Y. Lin, Graphene and graphene oxide: biofunctionalization and applications in biotechnology, *Trends in Biotechnology* **29** (2011) 205-212. https://doi.org/10.1016/j.tibtech.2011.01.008
[15] F. Liu, J. Y. Choi, T. S. Seo, Graphene oxide arrays for detecting specific DNA hybridization by fluorescence resonance energy transfer, *Biosensors and Bioelectronics* **25** (2010) 2361-2365. https://doi.org/10.1016/j.bios.2010.02.022
[16] C.-H. Lu, H.-H. Yang, C.-L. Zhu, X. Chen, G.-N. Chen, A graphene platform for sensing biomolecules, *Angewandte Chemie International Edition* **48** (2009) 4785-4787. https://doi.org/10.1002/anie.200901479
[17] Y. Zhang, Z.-R. Tang, X. Fu, Y.-J. Xu, TiO_2-graphene nanocomposites for gas-phase photocatalytic degradation of volatile aromatic pollutant: is TiO_2-graphene truly different from other TiO_2-carbon composite materials?, *ACS Nano* **4** (2010) 7303-7314. https://doi.org/10.1021/nn1024219
[18] M. Zhou, Y. Zhai, S. Dong, Electrochemical sensing and biosensing platform based on chemically reduced graphene oxide, *Analytical Chemistry* **81** (2009) 5603-5613. https://doi.org/10.1021/ac900136z
[19] A. J. Bard, L. R. Faulkner, *Electrochemical Methods: Fundamentals and Applications*, 2nd ed., Wiley, New York, USA, 2001, p. 833. ISBN 978-0-471-04372-0
[20] K. C. Honeychurch, Voltammetric behaviour of rhodamine B at a screen-printed carbon electrode and its trace determination in environmental water samples, *Sensors* **22** (2022) 4631. https://doi.org/10.3390/s22124631
[21] X. An, J. C. Yu, Graphene-based photocatalytic composites, *RSC Advances* **1** (2011) 1426-1434. https://doi.org/10.1039/c1ra00382h
[22] Q. Xiang, J. Yu, M. Jaroniec, Graphene-based semiconductor photocatalysts, *Chemical Society Reviews* **41** (2012) 782-796. https://doi.org/10.1039/c1cs15172j

[23] S. He, B. Song, D. Li, C. Zhu, W. Qi, Y. Wen, L. Wang, S. Song, H. Fang, C. Fan, A graphene nanoprobe for rapid, sensitive, and multicolor fluorescent DNA analysis, *Advanced Functional Materials* **20** (2010) 453-459. https://doi.org/10.1002/adfm.200901639
[24] S. Srivastava, T. D. Senguttuvan, B. K. Gupta, Highly efficient fluorescence quenching with chemically exfoliated reduced graphene oxide, *Journal of Vacuum Science & Technology B* **36** (2018) 04G104. https://doi.org/10.1116/1.5026170
[25] X. Xiao, Y. Zhang, L. Zhou, B. Li, L. Gu, Photoluminescence and fluorescence quenching of graphene oxide: a review, *Nanomaterials* **12** (2022) 2444. https://doi.org/10.3390/nano12142444
[26] Y. Wang, Z. Li, D. Hu, C. T. Lin, J. Li, Y. Lin, Aptamer/graphene oxide nanocomplex for in situ molecular probing in living cells, *Journal of the American Chemical Society* **132** (2010) 9274-9276. https://doi.org/10.1021/ja103169v
[27] C. N. R. Rao, A. K. Sood, K. S. Subrahmanyam, A. Govindaraj, Graphene: the new two-dimensional nanomaterial, *Angewandte Chemie International Edition* **48** (2009) 7752-7777. https://doi.org/10.1002/anie.200901678
[28] Q. Mei, K. Zhang, G. Guan, B. Liu, S. Wang, Z. Zhang, Highly efficient photoluminescent graphene oxide with tunable surface properties, *Chemical Communications* **46** (2010) 7319-7321. https://doi.org/10.1039/c0cc02374d
[29] J. I. Paredes, S. Villar-Rodil, A. Martínez-Alonso, J. M. D. Tascón, Graphene oxide dispersions in organic solvents, *Langmuir* **24** (2008) 10560-10564. https://doi.org/10.1021/la801744a
[30] M. Pumera, Electrochemistry of graphene, graphene oxide and other graphenoids: review, *Electrochemistry Communications* **36** (2013) 14-18. https://doi.org/10.1016/j.elecom.2013.08.028
[31] D. Chen, L. Tang, J. Li, Graphene-based materials in electrochemistry, *Chemical Society Reviews* **39** (2010) 3157-3180. https://doi.org/10.1039/b923596e
[32] Y. Shao, J. Wang, H. Wu, J. Liu, I. A. Aksay, Y. Lin, Graphene based electrochemical sensors and biosensors: a review, *Electroanalysis* **22** (2010) 1027-1036. https://doi.org/10.1002/elan.200900571
[33] Q. He, J. Liu, Y. Tian, Y. Wu, F. Magesa, P. Deng, G. Li, Facile preparation of Cu_2O nanoparticles and reduced graphene oxide nanocomposite for electrochemical sensing of rhodamine B, *Nanomaterials* **9** (2019) 958. https://doi.org/10.3390/nano9070958
[34] A. E. Kartika, H. Setiyanto, R. V. Manurung, S. N. A. Jenie, V. Saraswaty, Silver nanoparticles coupled with graphene nanoplatelets modified screen-printed carbon electrodes for rhodamine B detection in food products, *ACS Omega* **6** (2021) 31477-31484. https://doi.org/10.1021/acsomega.1c03414
[35] I. V. Lightcap, T. H. Kosel, P. V. Kamat, Anchoring semiconductor and metal nanoparticles on a two-dimensional catalyst mat. Storing and shuttling electrons with reduced graphene oxide, *Nano Letters* **10** (2010) 577-583. https://doi.org/10.1021/nl9035109
[36] P. V. Kamat, Graphene-based nanoarchitectures. Anchoring semiconductor and metal nanoparticles on a two-dimensional carbon support, *The Journal of Physical Chemistry Letters* **1** (2010) 520-527. https://doi.org/10.1021/jz9001642
[37] L. Jing, Y. Qu, B. Wang, S. Li, B. Jiang, L. Yang, W. Fu, H. Fu, J. Sun, Review of photoluminescence performance of nano-sized semiconductor materials and its relationships with photocatalytic activity, *Solar Energy Materials and Solar Cells* **90** (2006) 1773-1787. https://doi.org/10.1016/j.solmat.2005.11.007
[38] M. Golestaneh, Applicability of a graphene oxide nanocomposite for fabrication of an electrochemical sensor for simultaneous detection of sunset yellow and rhodamine B in food samples, *Analytical Methods* **15** (2023) 5500-5509. https://doi.org/10.1039/d3ay01373a

CC BY

[39] D. Rehm, A. Weller, Kinetics of fluorescence quenching by electron and H-atom transfer, *Israel Journal of Chemistry* **8** (1970) 259-271. https://doi.org/10.1002/ijch.197000029
[40] J. R. Lakowicz, *Principles of Fluorescence Spectroscopy*, 3rd ed., Springer, New York, USA, 2006, Chapter 8. https://doi.org/10.1007/978-0-387-46312-4_8
[41] K. F. Chou, A. M. Dennis, Förster resonance energy transfer between quantum dot donors and quantum dot acceptors, *Sensors* **15** (2015) 13288-13325. https://doi.org/10.3390/s150613288
[42] A. L. Eckermann, D. J. Feld, J. A. Shaw, T. J. Meade, Electrochemistry of redox-active self-assembled monolayers, *Coordination Chemistry Reviews* **254** (2010) 1769-1802. https://doi.org/10.1016/j.ccr.2009.12.023

©2026 by the authors; licensee IAPC, Zagreb, Croatia. This article is an open-access article distributed under the terms and conditions of the Creative Commons Attribution license (http://creativecommons.org/licenses/by/4.0/)